Journal of Applied Electrochemistry **29**: 855–860, 1999.

Physical and electrochemical characteristics of aluminium-substituted nickel hydroxide

B. LIU*, X.Y. WANG, H.T. YUAN, Y.S. ZHANG, D.Y. SONG and Z.X. ZHOU
Institute of New Energy Material Chemistry, Nankai University, Tianjin 300071, China
*(*author for correspondence, e-mail: bingliu@tju.edu.cn; fax: +86 22 23502604)*

Received 21 July 1998; accepted in revised form 12 January 1999

Key words: aluminium-substituted nickel hydroxide, reversibility, stability structure, utilization of active material

Abstract

Substitution of 20% aluminium for nickel in the lattice of nickel hydroxide, prepared by coprecipitation, leads to a hydrotalcite-like compound of formula $Ni_{0.8}Al_{0.2}(OH)_2(CO_3)_{0.1}.0.66\ H_2O$. It has been found that the compound has prolonged stability in 6 M KOH solution and can be used as the positive electrode material in rechargeable alkaline batteries. The structure, morphology and composition of the compound have been investigated by X-ray diffraction, scanning electron microscopy and infrared spectroscopy. The electrode comprising the aluminium-substituted nickel hydroxide has greater discharge capacity and higher utilization of active material than the β-$Ni(OH)_2$ electrode. Cyclic voltammetry suggest that the aluminium-substituted nickel hydroxide has better reversibility of the $Ni(OH)_2$/NiOOH redox couple and higher oxygen evolution overpotential than β-$Ni(OH)_2$. The mechanism of the electrode reaction has also been discussed and the proton diffusion coefficient in the compound has been determined.

1. Introduction

Nickel hydroxide has been extensively used as an active material of the positive electrode in rechargeable alkaline batteries, such as Ni/Cd, Ni/Fe, Ni/Zn, Ni/H_2 or Ni/metal hydride batteries. The overall reaction related to the $Ni(OH)_2$/NiOOH redox couple in alkaline electrolytes is

$$Ni(OH)_2 \leftrightarrow NiOOH + H^+ + e^- \quad (1)$$

The nickel hydroxide used as the nickel electrode can exist under two polymorphs denoted α and β. Both structures consist of brucite-type layers well ordered along the *c*-axis (β-phase) or randomly stacked along the *c*-axis (α-phase) with, for the latter, water molecules and anionic species within the Van der Waals gap resulting in a *c*-spacing of 7.5 Å compared to 4.8 Å for the β-phase [1]. Usually, the β-(II)/β(III) phases are the classical materials involved during electrode cycling. However, the α-$Ni(OH)_2$ phase materials have potential as active materials for nickel hydroxide electrodes [2]. It is well known that α-hydroxide, on oxidation, is converted to γ-NiOOH at a lower potential than the corresponding oxidation state compared with β-$Ni(OH)_2$ to β-NiOOH [3]. Since γ-NiOOH has a higher average nickel oxidation state compared with β-NiOOH, the capacity of the α/γ system is better than that of β(II)/β(III). The α and γ phases are hydrated, α-$Ni(OH)_2$ can also be cycled to the γ-NiOOH phase reversibly without any mechanical deformation and the mechanical constraints that occur during cycling are reached [4]. Unfortunately, α-$Ni(OH)_2$ reverts to β-$Ni(OH)_2$ on standing in alkaline media. Thus, stabilization of α-$Ni(OH)_2$ in alkaline media is an important goal for potential application.

To enhance the stability of cycling between α-$Ni(OH)_2$ and γ-NiOOH, many studies of the partial substitution of metal ion for nickel in the lattice of nickel hydroxide have been carried out. Recently, Faure et al. [5] reported that cobalt substituted α-$Ni(OH)_2$, obtained by precipitation techniques, have been used as positive electrodes in Ni/Cd batteries; the results showed that these materials were stable in KOH solution and the electrochemical cycling between the α and γ phases allowed up to 1.3 e^- per (Ni + Co) atom to be reversibly exchanged

at the $C/5$ rate. Armstrong and Charles confirmed that a large cobalt addition to the nickel hydroxide (45%) allows stabilization of the γ/α cycling [6]. Ezhov et al. found that zinc addition could stabilize the thermodynamically unstable α-$Ni(OH)_2$ [7]. Demourgues et al. proposed the partial substitution of Co and Fe for nickel in nickel hydroxide to stabilize the cycling between α-$Ni(OH)_2$ and γ-NiOOH [8, 9]. The α-$Ni(OH)_2$ was stabilized by electrostatic interactions between Fe^{3+} or Co^{3+} substitution cations within the slab and the CO_3^{2-} ions that were inserted in the interslab space to compensate for the positive charge excess due to the trivalent state of the substituting cations. More recently, the chemical and physical properties of new manganese-substituted nickel hydroxide with interlamellar water prepared by precipitation have also been reported [10–12]. These materials exhibit the following general formula, strongly related to that of the hydrotalcites, or from a more general viewpoint, to that of the double hydroxides layer(LDHs):

$$\underset{\text{slab}}{[Ni^{II}_{1-y}Mn^{III}_{y}(OH)_2]^{y+}}\ \underset{\text{interslab space}}{[CO_3]^{y-}_{y/2}\ [H_2O]_z}$$

Kamath et al. have synthesized the hydrotalcite-like compound of formula $Ni_{1-x}Al_x(OH)_2\ (CO_3)_{x/2}.nH_2O$ ($x = 0.1$ to 0.25) by substitution of nickel hydroxide by aluminium and found that the compounds of compositions $x \geqslant 0.2$ have prolonged stability in strongly alkaline medium [13]. The electrode, comprising stabilized α-$Ni(OH)_2$ of $x = 0.2$ composition, is rechargeable with discharge capacity values of 240 ($\pm$ 15) mA h g^{-1}. Armstrong et al. studied the charge–discharge behaviour of hydrated aluminium-substitution nickel hydroxide in Ni/Cd batteries and showed that the nickel electrode, comprising nickel hydroxide, had a relatively higher discharge potential plateau and relatively greater discharge capacity [14]. In the present paper, we describe the synthesis of aluminium stabilized α-$Ni(OH)_2$ by chemical coprecipitation and discuss its physical and electrochemical properties; moreover, we also use this compound as electrode material for high performance nickel positive electrodes in Ni/MH batteries.

2. Experimental details

2.1. *Preparation of samples*

The aluminium stabilized α-$Ni(OH)_2$ samples were prepared at room temperature by adding a mixed solution containing $NiSO_4.6\ H_2O$ and $Al_2(SO_4)_3.18\ H_2O$ in the required stoichiometric ratio to 1 M NaOH solution containing an appropriate amount of Na_2CO_3. A green precipitate was obtained which was washed in distilled water and centrifuged several times until the pH became neutral. The precipitate was dried at 65 °C.

2.2. *Analysis*

The morphology of aluminium stabilized α-$Ni(OH)_2$ was examined using scanning electron microscopy (SEM) (Hitachi X-650 type). Structures were determined using X-ray diffraction (XRD) (D/Max-IIIA X-ray diffractometer, Rigaku Ltd, Japan), CuK_α radiation and a nickel filter at 35 kV and 40 mA. A study of the sample was performed by infrared spectroscopy using a Nicolet 510 Fourier transform infrared (FTIR) spectrophotometer.

2.3. *Electrode preparation*

Electrode substrates were prepared from a 1 cm $\times$ 1 cm square thin sheet of nickel foam. At first, the aluminium stabilized nickel hydroxide powder was mixed with 10% cobalt oxide powder; then the appropriate amount of polytetrafluoroethylene (PTFE) aqueous suspension as a binder was added and kneaded to obtain paste. The paste was incorporated into the nickel foam substrate using a spatula, dried at 60 °C for 1 h, and then pressed at 20 MPa for 1 min to assure good electrical contact between the subject and the active material.

Charge–discharge experiments were carried out using one nickel electrode coupled with two metal hydride (MH) electrodes ($Mm(NiCoMnAl)_5$, provided by our institute). The electrodes were protected by a separator. The electrolyte consisted of 6 M KOH + 15% LiOH. Charge was initially carried out at the $C/10$ rate for 150% theoretical capacity, held for 30 min; then the discharge was performed at the $C/5$ rate to 0.1 V vs Hg/HgO.

2.4. *Cycle voltammetric studies*

All cyclic voltammetric studies were performed in a three-compartment electrolysis cell at 25 °C using a 1287 electrochemical interface with a personal computer. The working electrodes were powder microelectrodes with diameter 150 μm. Two nickel sheet counterelectrodes were placed at the side and the working electrode was positioned in the centre. A Hg/HgO reference electrode was used with a lugging capillary in the region of the working electrode. The working electrodes were activated by repeated potential scan between 0 and 0.65 V vs Hg/HgO at the 10 mV s^{-1} rate 10 times prior to the experiments.

3. Results and discussion

The chemically prepared aluminium-substituted nickel hydroxide has the formula $Ni_{1-x}M^{III}_x(OH)_2A^{n-}_{x/n}.yH_2O$ [13]. In the present study, M is trivalent aluminium ion, A is CO_3^{2-}, x is 0.2 and y is 0.66. Thus, the aluminium-stabilized α-$Ni(OH)_2$ synthesized has the formula $Ni_{0.8}Al_{0.2}(OH)_2(CO_3)_{0.1}.0.66\ H_2O$.

The X-ray diffraction pattern of aluminium-stabilized α-$Ni(OH)_2$ is given in Figure 1 in comparison with that of the well known unsubstituted β-$Ni(OH)_2$. α-$Ni(OH)_2$ and β-$Ni(OH)_2$ crystallize in the hexagonal system with the brucite-type structure with $Ni(OH)_2$ layers stacked along the c axis. Each $Ni(OH)_2$ layer consists of a hexagonal planar arrangement of octahedrally oxygen coordinated Ni(II) ions. The main difference between the α-$Ni(OH)_2$ and β-$Ni(OH)_2$ forms resides in the stacking of the layers along the c-axis. β-$Ni(OH)_2$ layers are perfectly stacked along the c-axis with an interlamellar distance of 4.6 Å, but α-$Ni(OH)_2$ layers are randomly oriented and separated by intercalar water molecules bonded to the hydroxyl groups by hydrogen bonds [15]. The interlamellar distance for the α-$Ni(OH)_2$ is about 8 Å. It may be seen from Figure 1 that the XRD pattern of aluminium stabilized α-$Ni(OH)_2$ is apparently different from that of β-$Ni(OH)_2$, and is the same as that of unsubstituted α-$Ni(OH)_2$ reported in the literature [15, 16]. The XRD pattern of β-$Ni(OH)_2$ in Figure 1(b) shows lines at 4.64, 2.71, 2.31 and 1.75 Å, respectively. The XRD pattern of stabilized α-$Ni(OH)_2$ in Figure 1(a) has a completely different structure and show a low angle reflection close to 8 Å, followed by another at around 4 Å. The results are in agreement with values examined by Kamath [13] and Indira [17] for the layered double hydroxides (LDHs) of nickel with aluminium.

By scanning electron microscopy the aluminium stabilized nickel hydroxide appears as aggregates of thin crumpled sheets, with no definite shape (Figure 2(a)). This is a characteristic feature which has also been observed with unsubstited α-$Ni(OH)_2$. In addition, it has been found from Figure 2 that the morphology of

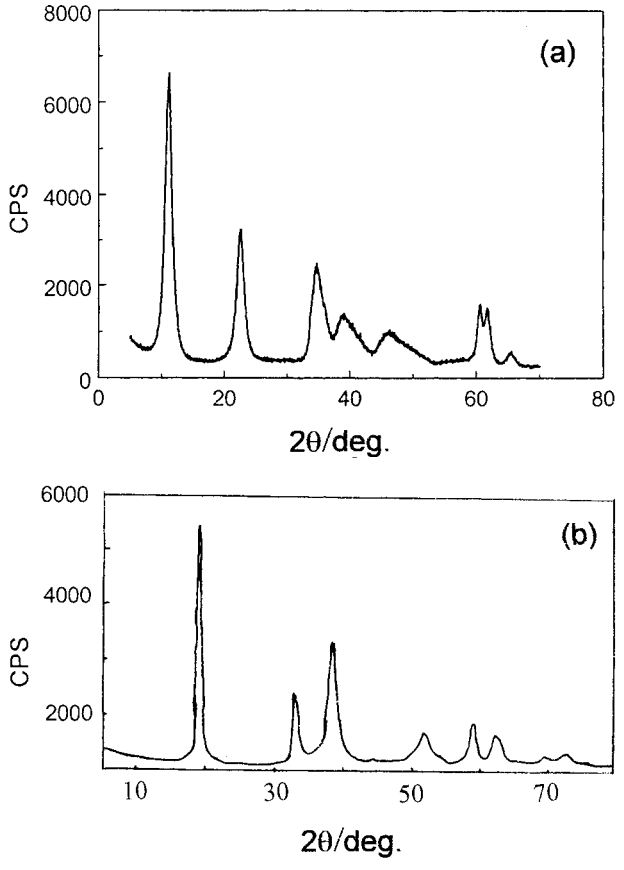

Fig. 1. X-ray diffraction patterns for (a) Al-stablized α-$Ni(OH)_2$, and (b) β-$Ni(OH)_2$.

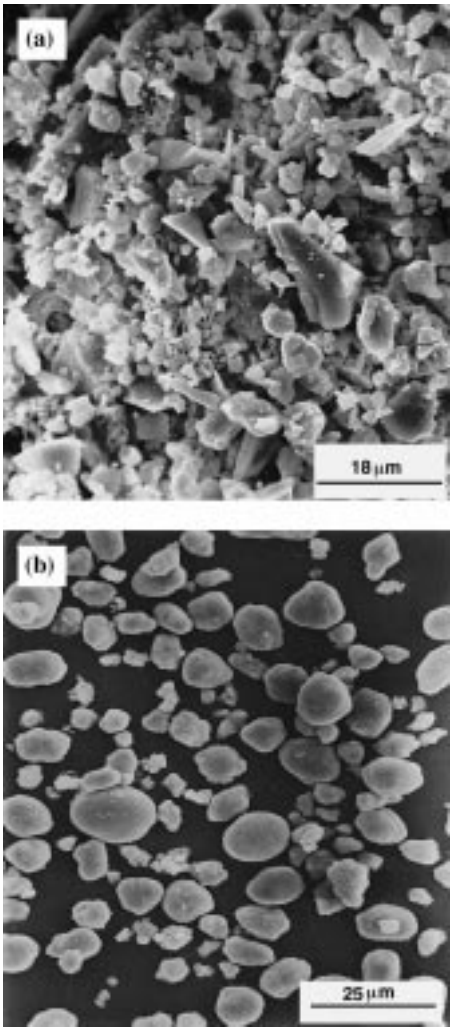

Fig. 2. SEM micrographs. see text. Scalebars: 2θ.

the aluminium stabilized α-$Ni(OH)_2$ (Figure 2(a)) is different from that of β-$Ni(OH)_2$ (Figure 2(b)), which showed spherical particles.

Infrared spectroscopy allows good characterization of α-$Ni(OH)_2$; the presence of inserted anions and hydrogen bonding (between the hydrogen atom of the OH groups and the oxygen atoms of intercalated anions or water molecules) can easily be detected. Figure 3 shows the IR spectrum of aluminium stabilized α-$Ni(OH)_2$. It is evident that the aluminium stabilized α-$Ni(OH)_2$ is similar to α-$Ni(OH)_2$. In the case of β-$Ni(OH)_2$, the narrow line at 3600 cm^{-1} can be attributed to 'free' OH groups and the shoulder in the 3000~3600 cm^{-1} range is characteristic of the presence of absorbed water molecules [15]. For the α-$Ni(OH)_2$, the narrow line at 3600 cm^{-1} has disappeared as all hydrogen atoms are hydrogen bonding (very large bond in the 2600~ 3600 cm^{-1} range). Moreover, α-$Ni(OH)_2$ also exhibits several bands in the range 1600–700 cm^{-1} which have been attributed to absorbed carbonate ions [4]. It can be clearly seen from Figure 3 that the IR spectrum of the aluminium stabilized α-$Ni(OH)_2$ exhibits strong similarities with that of unsubstituted α-$Ni(OH)_2$ as reported in the literature [2, 15]. The broad band centred about 3400 cm^{-1} is characteristic of the hydrogen-bonded hydroxyl group. Strong absorption in the 1600 to 1000 cm^{-1} region is due to intercalated anions. The band at 1377 cm^{-1} is due to CO_3^{2-} ions inserted in the α-$Ni(OH)_2$ interslab spaces; the CO_3^{2-} ions can compensate for the excess of positive charge due to the Al^{3+} within the slab. Two bonds seen in the 800 to 200 cm^{-1} range are due to the OH in the plane (721.9 cm^{-1}) and metal oxygen stretching (571.6 cm^{-1}) frequencies, respectively [17]. These features also have a remarkable similarity with the results reported by Indira et al. [17].

Figure 4 shows the discharge curve of a MH/Ni battery in which the positive electrode consists of aluminium stabilized nickel hydroxide. As seen from Figure 4, the discharge capacity of the positive electrode

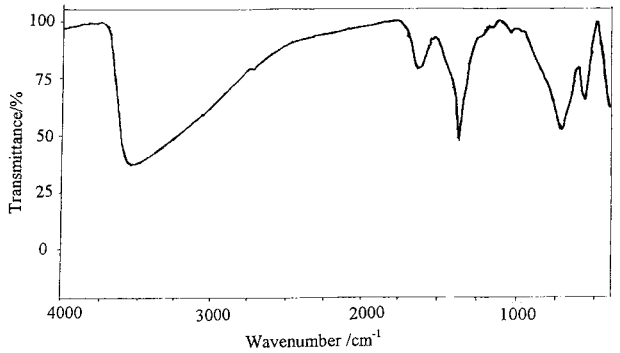

Fig. 3. IR spectroscopy of Al-stabilized α-$Ni(OH)_2$.

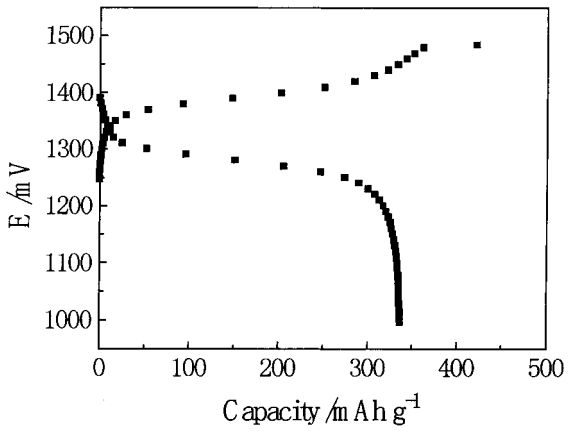

Fig. 4. The discharge curve of MH/Ni battery using the Al- stablized α-$Ni(OH)_2$ as positive.

is 340 mA h g^{-1}. In general, the theoretical capacity of β-$Ni(OH)_2$ is 289 mA h g^{-1} by assuming the electrode reaction to be

$$Ni(OH)_2 + OH^- \leftrightarrow NiOOH + H_2O + e^- \qquad (2)$$

As a consequence, it can be concluded that the aluminium stabilized α-$Ni(OH)_2$ has greater discharge capacity than the theoretical capacity of β-$Ni(OH)_2$. The reasons might be the discharge process, as the specific discharge capacity depends significantly on the phase composition. The discharge capacity, as a rule, is higher for electrodes containing γ-NiOOH, which is caused by a higher nickel oxidation state; in γ-NiOOH it can reach values close to 3.7 while for β-NiOOH it only slightly exceeds 3.0 [18]. While in the case of aluminium stabilized α-$Ni(OH)_2$ the phase transformation during charge–discharge cycle is α-$Ni(OH)_2 \leftrightarrow \gamma$-NiOOH, the exchange electrons per nickel atom are more than one. Thus, the electrode exhibits the greater discharge capacity.

As mentioned above, stabilization of α-$Ni(OH)_2$ in alkaline media is an important goal for future applications. Usually, α-$Ni(OH)_2$ has an unstable structure and reverts to β-$Ni(OH)_2$ on standing in alkali. Figure 5 shows variation of the discharge capacity with cycle number for aluminium stabilized α-$Ni(OH)_2$. The discharge capacity remains higher than the theoretical discharge capacity of β-NiOOH during the 40 cycles and stabilizes its discharge capacity at about 340 mA h g^{-1}. Consequently, we consider the aluminium stabilized α-$Ni(OH)_2(Ni_{0.8}Al_{0.2}(OH)(CO_3)_{0.1}.0.66\ H_2O)$ obtained by the present technique is stable during charge–discharge over several cycles. This is due to the fact that stabilization in α-$Ni(OH)_2$ arises from a double hydroxide which contains Al^{3+} substituted for Ni^{2+} in the nickel hydroxide lattice. The charge excess due to Al^{3+}

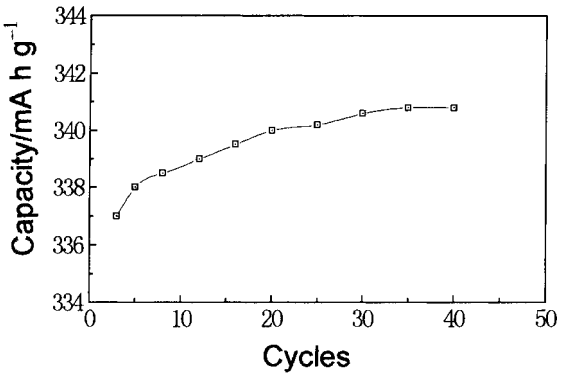

Fig. 5. Discharge curve with cycles for Al-stablized α-$Ni(OH)_2$.

are compensated by the insertion of carbonate between the hydroxide slabs (Figure 3). The anions strongly anchor the positive charged brucite layers and stabilize the structure in a variety of stressful condition [13]. α-$Ni(OH)_2$ is a pure divalent material and anion intercalation occurs more on account of hydroxyl ion vacancies rather than due to the exigencies of charge compensation. Thus, anion content is low and its bonding strength with the brucite layer is poor. This accounts for the poor stability of α-$Ni(OH)_2$ in alkaline media. Introducing Al into the nickel hydroxide lattice, not only enhances the intercalated anion contact, but also effectively stabilizes the α-$Ni(OH)_2$ structure in alkaline media [13].

Figure 6 shows the typical cyclic voltammograms of a microelectrode comprising aluminium stabilized α-$Ni(OH)_2$. In the range of scanning potentials employed, only one anodic oxidation peak, appearing at about 480 mV, was recorded prior to oxygen evolution. Similarly, only one oxyhydroxide reduction peak at about 380 mV was observed on the reverse sweep. The average peak potential, E_{rev}, is taken as an estimate of the reversible potential and the difference between the

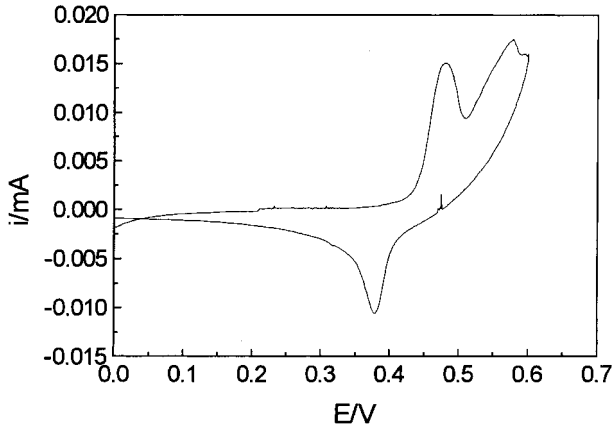

Fig. 6. Cyclic voltammograms of Al-stablized α-$Ni(OH)_2$.

anodic and cathodic peak position, $\Delta E_{a,c}$, is taken as an estimate of the reversibility of the redox reaction [19, 20]. Oxygen evolution is a parasitic reaction during charge of the nickel electrode. To compare the effect of aluminium stabilized α-$Ni(OH)_2$ on the oxygen evolution reaction, the difference between the oxidation peak potential and the oxygen evolution potential (DOP) [21] on the return sweep required to produce 1.5×10^{-5} A of anodic current is also estimated from the voltammograms. The results of the cyclic voltammetric studies in Figure 6 are tabulated in Table 1 in comparison with results for β-$Ni(OH)_2$ [22].

The results in Figure 6 and Table 1 illustrated that aluminium stabilized α-$Ni(OH)_2$ allows the electrode to charge at a significantly less positive potential (480 mV instead of 520 mV). In addition, the charge process appears to occur more reversibly ($\Delta E_{a,c}$ is 102 mV instead of 280 mV). Moreover, the oxygen evolution overpotential shifts to a more positive value. Thus, these results clearly indicate that this aluminium stabilized α-$Ni(OH)_2$ electrode allows the charge process to occur more easily and more reversibly, suggesting that much more active material can be utilized during charge. Due to the increase in the oxygen evolution overpotential and the decrease in the oxidation peak potential of nickel hydroxide, the charge efficiency of the electrode is also markedly improved, indicating that the electrode has greater discharge capacity. These results are in good agreement with those obtained by Corrigan et al.; they have reported that coprecipitation of cobalt or manganese in nickel hydroxide thin films decreases the oxidation potential with respect to that of the unsubstituted nickel hydroxide [20].

Typical cyclic voltammograms for an aluminium stabilized α-$Ni(OH)_2$ electrode at various scan rates are shown in Figure 7. Characteristic cyclic voltammetry parameters obtained from Figure 7 are shown in Figure 8 as a function of sweep rate. It can be seen that the cyclic voltammetric peak current, i_{pa}, against $v^{1/2}$ plot, where v is the potential scan rate, gives a reasonably linear relationship according to the classical Sevick equation. That is,

$$i_p = 2.69 \times 10^5 n^{3/2} A D_0^{1/2} v^{1/2} C_0 \quad (3)$$

Table 1. Results of cyclic voltammetry measurements

Electrode	E_{anodic} /mV	$E_{cathodic}$ /mV	$\Delta E_{a,c}$ /mV	E_{rev} /mV	DOP /mV
1	480	378	102	429	120
2	520	240	280	380	89

Note: 1. Aluminium stabilized α-$Ni(OH)_2$ 2. β-$Ni(OH)_2$ microencapsulated by 5% Co [21]

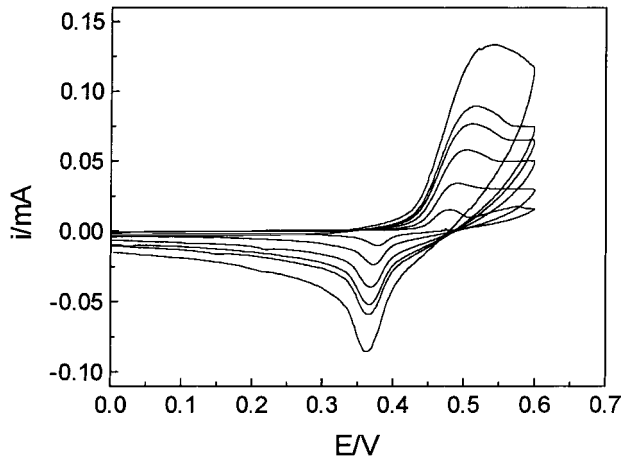

Fig. 7. Cyclic voltammograms of Al-stablized α-$Ni(OH)_2$ at various scan rate.

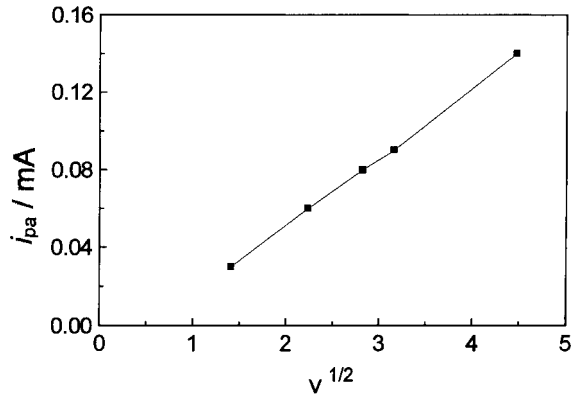

Fig. 8. The Relationship of ipa with $v^{1/2}$.

where n is the number of electrons transferred and n is 1.5 (chosen here). A is the real surface area of the electrode and has a value of 8×10^{-3} cm^2 as indicated by impedance measurements. D_0 is the diffusion coefficient of the rate limiting species (i.e., protons) and C_0 is the proton concentration, which is estimated by dividing the molecular weight of $Ni_{0.8}Al_{0.2}(OH)_2(CO_3)_2.0.66$ H_2O by its density. From Equation 3 and the slope of the i_{pa} against $v^{1/2}$ plot in Figure 8, we calculate that the proton diffusion coefficient in the aluminium stabilized α-$Ni(OH)_2$ electrode is 9.27×10^{-9} $cm^2\,s^{-1}$. Wang et al. [22] measured a diffusion coefficient of 1.2×10^{-9} $cm^2\,s^{-1}$ for a microenscopsulated cobalt β-$Ni(OH)_2$ electrode using cyclic voltammetry. Zhang et al. [23] reported a diffusion coefficient of 1.0×10^{-11} $cm^2\,s^{-1}$ for β-$Ni(OH)_2$ using the same technique. The present value is higher than that reported by both Wang [22] and Zhang [23]. The reason for such a high proton diffusion coefficient is the insertion of anions in the interslab.

4. Conclusion

(i) Aluminium stabilized α-$Ni(OH)_2$ has the same structure as that of α-$Ni(OH)_2$.
(ii) Due to an exchange of more than one electron during the charge–discharge cycle, the electrode has greater discharge capacity and higher utilization of active material.
(iii) Electrode reactions occurring at aluminium stabilized α-$Ni(OH)_2$ have a better redox reversibility; the oxygen evolution overpotential shifts to more positive values.
(iv) Due to the insertion of anions in the interslab, the electrode has relatively higher proton conductivity.

References

1. A. Audemer, A. Delahaye, R. Farhi, N.S. Epee and J.M. Tarascon, *J. Electrochem. Soc.* **144** (1997) 2614.
2. A.D. Vidal and M. Figlarz, *J. Appl. Electrochem.* **17** (1987) 589.
3. R. Barnard, C.F. Randell and F.L.Tye, *J. Appl. Electrochem.* **10** (1980) 127.
4. C. Delmas, C. Faure and Y. Borthomieu, *Mater. Sci. Eng. B* **13** (1992) 89
5. C. Faure, C. Delmas and P. Willmann, *J. Power Sources* **36** (1991) 497.
6. R.D. Armstrong and E.A. Charles, *J. Power Sources* **25** (1989) 89.
7. B.B. Ezhov and O.G. Malandin, *J. Electrochem. Soc.* **138** (1991) 885.
8. C. Faure, C. Pelmas and P. Willmann, *J. Power Sources*. **35** (1991) 263.
9. L.G. Demourgues, J.J. Braconnier and C. Delmas, *J. Power Sources* **45** (1993) 281.
10. L.G. Demourgues and C. Delmas, *J. Electrochem. Soc.* **143** (1996) 561.
11. L.G. Demourgues, C. Denage and C. Delmas, *J. Power Sources* **52** (1994) 269.
12. L.G. Demourtgues and C. Delmas, *J. Power Sources* **52** (1994) 275.
13. P.V. Kamath, M. Dixit, L. India, A.K. Shukla, V.G. Kumar and N. Munichandraiah, *J. Electrochem. Soc.* **141** (1994) 2956.
14. R.D. Armstrong and H. Wang, *Electrochim. Acta.* **36** (1991) 759.
15. P. Oliva, J. Leonardi, J.F. Laurent, C. Delmas, J.J. Braconnier, M. Figlarz and F. Fievet, *J. Power Sources* **8** (1982) 229.
16. M.C. Bernard, P. Bernard, M. Keddam, S. Senyarich and H. Takenouti, *Electrochim. Acta* **41** (1996) 91.
17. L. Indira, M. Dixit and P.V. Kammath, *J. Power Sources* **52** (1994) 93.
18. H. Bode, K. Dehmelt and J. Witle, *Z. Anorg. Chem.* **366** (1969) 1.
19. P.V. Kamath and M.F. Ahmed, *J. Appl. Electrochem.* **23** (1993) 225.
20. D.A. Corrigan and R.M. Bendert, *J. Electrochem. Soc.* **136** (1989) 723.
21. X. Wang, J. Yan, H. Yuan and Y. Zhang, *J. Power Sources* **72** (1998) 221.
22. X. Wang, J. Yan, H. Yuan and Y. Zhang, *J. Appl. Electrochem.* in press.
23. C. Zhang and S.M. Park, *J. Electrochem. Soc.* **134** (1987) 2966.